Title: mRNA structure determines specificity of a polyQ-driven phase separation

Authors: Erin M. Langdon[1], Peggy Billingsly[3], Amirhossein Ghanbari Niaki[3], Grace McLaughlin[1], Chase Weidmann[2], Therese Gerbich[1], Christina M. Termini[4], Kevin M. Weeks[2], Sua Myong[3] and Amy S. Gladfelter[1*]

Affiliations:

[1]Department of Biology
[2]Department of Chemistry
University of North Carolina at Chapel Hill
Chapel Hill, NC 27599
[3]Department of Biophysics
Johns Hopkins University
Baltimore, MD 21218
[4]Division of Hematology/Oncology, Department of Medicine
University of California, Los Angeles
Los Angeles, CA 90095
*Correspondence to: amyglad@unc.edu

Abstract:

Many subcellular structures assemble via liquid-liquid phase separation (LLPS) to form compartments without membranes. Though it has been shown that RNA is a central driver and modulator of LLPS, it is not yet known how these liquid droplets establish and maintain individual identities. Here we examine how mRNAs are recruited to or excluded from liquid compartments based on their sequence and ability to self-associate. We find that the specific secondary structure of a cyclin mRNA is required for it to assemble into distinct droplets and be excluded from other droplets containing functionally-unrelated mRNAs. This molecular mechanism explains how sequence-encoded shape information in RNA promotes the coexistence of the diverse array of RNA-rich liquid compartments found in a single cell.

One Sentence Summary:

Identity in cellular, phase-separated compartments emerges from RNA-RNA complexes encoded by mRNA secondary structures.

Main Text:

The formation of non-membrane bound organelles through the condensation of macromolecules is a newly appreciated mechanism of intracellular organization. These condensates often display liquid-like properties and form through liquid-liquid phase separation (LLPS) (*1*, *2*). The growing list of LLPS-assembled compartments includes the nucleolus, RNA granules, cell signaling hubs, the spindle matrix, chromatin, the synaptonemal complex, and many pathological neuronal granules (*3-12*). Despite the growing appreciation of the variety of liquid-like assemblies employed in diverse cellular processes, a fundamental unsolved problem is how liquid droplets recruit distinct constituents and retain independent identities, rather than fusing into a singular compartment. This is especially remarkable given the fact that many of the constituents are highly disordered proteins and the droplets they form display such a propensity to fuse (*2*). RNA has been shown to be a driver of LLPS and can modulate the material properties of droplets (*13-20*), yet there is little known about how RNA can impact the identity and maintenance of coexisting liquid compartments. Here we show that mRNA secondary structure is required for droplet identity and likely acts through higher-order interactions between mRNAs and RNA-binding proteins. This illustrates how molecular scale interactions can encode the identity and emergent properties of micron-scale liquid compartments in cells.

Whi3 is a polyQ-containing RNA-binding protein identified in *Saccharomyces cerevisiae* through its role in cell size control (*21*). Whi3 is known for its roles in morphogenesis, memory of mating, and stress responses, where the protein forms aggregates and associates with RNA-processing bodies (*22-26*). The homolog in the filamentous fungus *Ashbya gossypii* has an expanded polyQ tract, a sequence known to promote self-assembly and forms liquid-like droplets that function to locally regulate nuclear cycling and hyphal morphogenesis (*27*, *28*). In vitro, Whi3 polyQ-dependent LLPS is driven by the presence of specific RNAs encoding regulators of either the cell cycle (e.g. the cyclin *CLN3*) or actin (e.g. the formin *BNI1*) (*14*). We see two distinct types of Whi3 droplets in *Ashbya* cells: droplets clustered around nuclei where *CLN3* mRNAs are positioned and droplets at growing cell tips where *BNI1* mRNAs are localized (Fig. 1A, movie S1, (*27*, *28*)). These different droplets have different amounts of Whi3 (Fig. 1B) and different rates of Whi3 incorporation based on accumulation of Whi3-Halo, visualized after a pulse of dye (Fig. 1C). These differences suggest Whi3 droplets around nuclei and at tips are somehow structurally distinct.

The distinct droplet properties in cells may depend on extrinsic features of the local cytosolic microenvironment near nuclei and at tips or may arise due to the presence of different constituents within the droplets. *CLN3* and *BNI1* mRNAs did not co-localize in the cytoplasm as assessed by smRNA F.I.S.H., although they were co-expressed by the same nuclei ~20% of the time, shown by bright signals within the same nucleus (Fig. 1, D and F). This suggests that there are intrinsic, compositional differences between droplets and that the components are mutually exclusive. In contrast, *SPA2* mRNA, another Whi3-interacting partner that encodes a different cell polarity regulator, did frequently co-localize with *BNI1* mRNAs especially at growth sites

(Fig. 1, D and F) indicating that Whi3 droplets can contain mRNAs with different sequences. Thus, mRNAs encoding functionally-related proteins co-localize while functionally unrelated mRNAs bound by Whi3 do not. How can distinct Whi3-binding mRNAs segregate to different droplets in a common cytoplasm?

To address this question, we tested if the mRNA sequence alone was sufficient to generate individuality in droplets in a minimal reconstitution system of pure Whi3 protein and cyclin and formin mRNAs. In vitro, similarly as seen in cells, Whi3 droplets made out of *BNI1* mRNA were more enriched in Whi3 protein than droplets made with *CLN3* mRNA and accumulated more protein with time (Fig. S1A). Remarkably, when *CLN3* mRNA is added to Whi3 droplets made with *BNI1* mRNA (Fig. 2A), *CLN3* mRNA preferentially assembled into new, distinct droplets that did not fuse with the droplets containing *BNI1* mRNA (Fig. 2, B and C). In contrast, labeled *BNI1* mRNA readily incorporated into the droplets made of *BNI1* mRNA (Fig. 2, B and C). Notably, labeled *SPA2* mRNA also incorporated into *BNI1* droplets (Fig. 2, B and C). *CLN3* mRNAs also preferentially assembled new droplets instead of being incorporated into *SPA2* droplets (Fig. S1B). Similar results were obtained when droplets were assembled in concentrated fungal cell extract (Fig. S1C). Thus, as seen in cells, *CLN3* and *BNI1*/*SPA2* mRNAs assemble into distinct droplets in vitro, suggesting that droplet identity is encoded by the mRNA.

The mRNA sequences could control the identity of droplets by favoring homotypic or specific heterotypic interactions between RNA molecules. To test for specific RNA-RNA interactions, we incubated RNAs with polyvalent cations in the absence of Whi3 to induce electrostatic mediated phase transition of the mRNAs (*29*). The mRNAs by themselves were all are capable

of homotypic assembly into either liquid or gel-like droplets (Fig. 2D). Strikingly, *CLN3* mRNAs had only minimal co-localization with *BNI1* or *SPA2* mRNAs, whereas *BNI1* and *SPA2* mRNAs had significantly more co-localization with each other than *CLN3* had with either mRNA associated with cell polarity (Fig. 2E). Thus, sequence-based features of the mRNA can underpin the assembly of distinct, immiscible structures.

We next investigated what features of the mRNA sequence generate specificity. An mRNA with a scrambled *CLN3* coding sequence (*cln3* scr) but identical nucleotide composition and Whi3 binding sites formed Whi3 droplets (Fig. S2A) but no longer showed any droplet specificity (Fig. 3, A and B). Given that the charge, length, nucleotide composition and number of Whi3 binding site number (valency) were identical in this construct, we hypothesized that the secondary structure of the mRNA was responsible for droplet specificity. When *CLN3* mRNA was heated to 95ºC to completely disrupt secondary structure, and then immediately added to Whi3-*BNI1* droplets, this "melted" mRNA readily incorporated into *BNI1* droplets (Fig. 3, A and B). When melted *CLN3* mRNA was slowly refolded using step-wise temperature changes, the "refolded" *CLN3* mRNA showed significantly less mixing than melted *CLN3* mRNA, but more mixing than native *CLN3* mRNA (Fig. 3B). Thus, specificity information in *CLN3* mRNA can be eliminated by scrambling the sequence outside of Whi3 binding sites or by disrupting secondary structure without introducing any changes to the RNA sequence.

What exact features of *CLN3* mRNA secondary structure promote specificity? We performed SHAPE-MaP, a method that uses a small electrophilic molecule to modify nucleotides in regions that are highly flexible, followed by reverse transcription to detect modified nucleotides and

sequence changes, and deep sequencing to identify structured RNA regions. (*30*, *31*). SHAPE-MaP was carried out on untreated *CLN3*, refolded *CLN3*, and *cln3* scrambled mRNA to evaluate differences in secondary structure (Fig. 3C, S2, B and C). Many of the first 400 nucleotides in the *CLN3* sequence have low SHAPE reactivity and low Shannon entropy (Fig. S2D, purple shaded regions), suggesting a high frequency of paired nucleotides and a highly-folded, secondary structure. This region was one of the most changed in the refolded *CLN3* sequence, with a statistically significant increase in SHAPE reactivity compared to the native *CLN3* sequence (Wilcoxon rank sum test, $p < 0.001$), as many nucleotides that were originally less reactive became more reactive (Fig. 3C, S2, B and D), suggesting that this region transitioned to a more unstructured state during the refolding process. These data suggest that melting and refolding allows the RNA to sample conformations that are significantly different from the structures formed during transcription. The *cln3* scrambled sequence showed an almost completely different SHAPE profile with dramatically altered secondary structure throughout the sequence (Fig. 3, C and D, Fig. S2C). Thus, secondary structure perturbations accompany the loss of droplet specificity.

One hypothesis to explain how RNA secondary structure might impact droplet specificity is that stem-loop elements might selectively display or mask sequences capable of base-pairing with other RNAs. The *CLN3* sequence contains five regions capable of heterotypic base-pairing with *BNI1* sequences (Fig. S3A). Most of these regions were located in areas of low SHAPE reactivity and thus more structured regions (Fig. S3B), suggesting that in the native *CLN3* RNA these complementary regions are relatively inaccessible for base pairing with *BNI1*. However, when the *CLN3* mRNA is melted, these regions might become available to base-pair with

complementary sequences on *BNI1*, providing a possible explanation for the structure-dependent loss of droplet specificity.

A striking difference in the structures between melted, scrambled, and untreated *CLN3* RNAs was the position of Whi3 binding sites relative to topological features such as stem-loops (Fig. 3D). In the untreated *CLN3*, three of the four Whi3 binding sites occurred in or overlapped single-stranded loops, whereas after melting and refolding, these sites were no longer in the same accessible context but rather found in stems, which may be less accessible to Whi3-binding. In *cln3*-scr, the Whi3 sites were also rearranged and instead incorporated into a single, extended run of stem-loops (Fig. 3D). Thus, in addition to biasing specific RNA-RNA interactions, RNA secondary structure may also influence how Whi3 interacts with target RNAs. This idea prompted us to examine roles for Whi3-binding to different RNAs in maintaining droplet specificity.

We found that a mutant of the *cln3* RNA (*cln3* 5m) in which the binding sites for Whi3 were altered no longer nucleated Whi3 droplets (Fig. S4A). Remarkably, however, *cln3* 5m nevertheless incorporated into Whi3-*BNI1* droplets (Fig. 4A). Interestingly, this mutant RNA had an appreciably different secondary structure from wild-type *CLN3* (Fig. S4, B and C), despite containing only five interspersed point mutations. To determine if Whi3 binding alters RNA conformation, we used single-molecule FRET (smFRET) to sample the conformational dynamics of *CLN3* and *BNI1* RNAs in the presence and absence of Whi3 (*32*). Fragments of *CLN3* or *BNI1* mRNA were labeled with donor fluorophores and hybridized to an 18 nt oligo with an acceptor fluorophore bound to a coverslip (Fig 4B). In the absence of protein, *CLN3*

RNA showed high FRET values indicative of a compacted state where donor and acceptor are in close proximity, while *BNI1* RNA showed a broader distribution of and somewhat lower FRET values, indicating a less compact state (Fig. 4C, purple shaded regions). Upon addition of Whi3, *CLN3* RNA FRET values decreased, indicating more extended RNA conformations were induced from the RNA-alone condition. In contrast, *BNI1* RNA showed a more substantial broadening of FRET values when complexed with Whi3 than *CLN3* (Fig. 4, C and D) suggesting that Whi3-*BNI1* complex is more dynamic. Dwell-time analysis, which measures the time between minimum FRET values, revealed that the Whi3-induced dynamics are over three times faster for *BNI1* than *CLN3* (Fig. 4D). These differences in FRET behavior show that different mRNAs react differentially in their intramolecular fluctuations to the presence of Whi3 providing a second layer of distinction amongst the droplets made with different RNAs.

Our findings suggest that Whi3 binding alters the conformational dynamics of target RNAs. We speculate that this could lead to a form of kinetic sorting, that serves to maintain droplet identities. In this model, the slower fluctuations of *CLN3* bound to Whi3 may be one source of exclusion from the more rapidly fluctuating *BNI1*-Whi3 complexes. Such altered dynamics might also drive the droplet-specific, emergent material properties (viscosity and surface tension) that we reported previously (*14*) and that may also serve as barriers to homogenization.

We show here that RNA secondary structure, derived from mRNA sequence and protein interactions, encodes a key level of specificity in the incorporation into liquid droplet compartments. We hypothesize that RNA secondary structures have been optimized to promote particular RNA-RNA interactions and the selective uptake of distinct RNAs and protein

constituents into droplets. Furthermore, protein binding to different sequences can lead to varied dynamics of complexes (Fig. 4E). We hypothesize that these different RNA conformation dynamics are another feature promoting immiscibility of coexisting droplets. Our findings indicate how specificity in RNA recruitment can be achieved in intracellular biological condensates and show that mRNAs can encode this specificity in their secondary structure. Given the large number of distinct RNA-based liquid bodies in a single cell, these mechanisms are likely broadly relevant to explain how droplets achieve and retain individuality.

References and Notes:

1. A. A. Hyman, C. A. Weber, F. Jülicher, Liquid-Liquid Phase Separation in Biology. *Annu. Rev. Cell Dev. Biol.* **30**, 39–58 (2014).

2. S. F. Banani, H. O. Lee, A. A. Hyman, M. K. Rosen, Biomolecular condensates: organizers of cellular biochemistry. *Nature Publishing Group*. **18**, 285–298 (2017).

3. S. C. Weber, C. P. Brangwynne, Inverse Size Scaling of the Nucleolus by a Concentration-Dependent Phase Transition. *Current Biology*. **25**, 641–646 (2015).

4. Y. Lin, D. S. W. Protter, M. K. Rosen, R. Parker, Formation and Maturation of Phase-Separated Liquid Droplets by RNA-Binding Proteins. *Molecular Cell*. **60**, 208–219 (2015).

5. A. Molliex *et al.*, Phase Separation by Low Complexity Domains Promotes Stress Granule Assembly and Drives Pathological Fibrillization. *Cell*. **163**, 123–133 (2015).

6. M. Zeng *et al.*, Phase Transition in Postsynaptic Densities Underlies Formation of Synaptic Complexes and Synaptic Plasticity. *Cell*. **166**, 1163–1175.e12 (2016).

7. X. Su *et al.*, Phase separation of signaling molecules promotes T cell receptor signal transduction. *Science*. **352**, 595–599 (2016).

8. S. Banjade, M. K. Rosen, Phase transitions of multivalent proteins can promote clustering of membrane receptors. *eLife*. **3**, 641–24 (2014).

9. H. Jiang *et al.*, Phase Transition of Spindle-Associated Protein Regulate Spindle Apparatus Assembly. *Cell*. **163**, 108–122 (2015).

10. A. R. Strom *et al*., Phase separation drives heterochromatin domain formation. *Nature*. **547**, 241–245 (2017).

11. O. Rog, S. Kohler, A. F. Dernburg, The synaptonemal complex has liquid crystalline properties and spatially regulates meiotic recombination factors. *eLife*, 1–26 (2017).

12. Y. Shin, C. P. Brangwynne, Liquid phase condensation in cell physiology and disease. *Science*. **357**, eaaf4382–13 (2017).

13. J. C. Schwartz, X. Wang, E. R. Podell, T. R. Cech, RNA Seeds Higher-Order Assembly of FUS Protein. *CellReports*. **5**, 918–925 (2013).

14. H. Zhang *et al*., RNA Controls PolyQ Protein Phase Transitions. *Molecular Cell*. **60**, 220–230 (2015).

15. S. Saha *et al*., Polar Positioning of Phase-Separated Liquid Compartments in Cells Regulated by an mRNA Competition Mechanism. *Cell*. **166**, 1572–1584.e16 (2016).

16. J. Smith *et al*., Spatial patterning of P granules by RNA- induced phase separation of the intrinsically-disordered protein MEG-3. *eLife*, 1–18 (2017).

17. X. Zhang *et al*., RNA stores tau reversibly in complex coacervates. *PLoS Biol*. **15**, e2002183–28 (2017).

18. S. Elbaum-Garfinkle *et al*., The disordered P granule protein LAF-1 drives phase separation into droplets with tunable viscosity and dynamics. *Proc Natl Acad Sci USA*. **112**, 7189–7194 (2015).

19. M. Feric *et al*., Coexisting Liquid Phases Underlie Nucleolar Subcompartments. *Cell*, 1–13 (2016).

20. A. Khong *et al*., The Stress Granule Transcriptome Reveals Principles of mRNA Accumulation in Stress Granules. *Molecular Cell*. **68**, 808–820.e5 (2017).

21. R. S. Nash, T. Volpe, B. Futcher, Isolation and Characterization of WHI3, a Size-Control Gene of Saccharomyces cerevisiae. *Genetics*, 1–12 (2001).

22. N. Colomina, F. Ferrezuelo, E. Vergés, M. Aldea, E. Garí, Whi3 regulates morphogenesis in budding yeast by enhancing Cdk functions in apical growth. *Cell Cycle*. **8**, 1912–1920 (2014).

23. S. Schladebeck, H.-U. Mosch, The RNA-Binding Protein Whi3 Is a Key Regulator of Developmental Signaling and Ploidy in Saccharomyces cerevisiae. *Genetics*, 1–22 (2013).

24. F. Caudron, Y. Barral, A Super-Assembly of Whi3 Encodes Memory of Deceptive Encounters by Single Cells during Yeast Courtship. *Cell*. **155**, 1244–1257 (2013).

25. G. Schlissel, M. K. Krzyzanowski, F. Caudron, Y. Barral, J. Rine, Aggregation of the

Whi3 protein, not loss of heterochromatin, causes sterility in old yeast cells. *Science*, 1–5 (2017).

26. K. J. Holmes, D. M. Klass, E. L. Guiney, M. S. Cyert, Whi3, an S. cerevisiae RNA-Binding Protein, Is a Component of Stress Granules That Regulates Levels of Its Target mRNAs. *PLoS ONE*. **8**, e84060–14 (2013).

27. C. Lee *et al*., Protein Aggregation Behavior Regulates Cyclin Transcript Localization and Cell-Cycle Control. *DEVCEL*. **25**, 572–584 (2013).

28. C. Lee, P. Occhipinti, A. S. Gladfelter, PolyQ-dependent RNA–protein assemblies control symmetry breaking. *J Cell Biol*. **208**, 533–544 (2015).

29. A. Jain, R. D. Vale, RNA phase transitions in repeat expansion disorders. *Nature*. **546**, 243–247 (2017).

30. M. J. Smola, G. M. Rice, S. Busan, N. A. Siegfried, K. M. Weeks, Selective 2′-hydroxyl acylation analyzed by primer extension and mutational profiling (SHAPE-MaP) for direct, versatile and accurate RNA structure analysis. *Nat Protoc*. **10**, 1643–1669 (2015).

31. M. J. Smola *et al*., SHAPE reveals transcript-wide interactions, complex structural domains, and protein interactions across the XistlncRNA in living cells. *Proc Natl Acad Sci USA*. **113**, 10322–10327 (2016).

32. Y. Kim, S. Myong, RNA Remodeling Activity of DEAD Box Proteins Tuned by Protein Concentration, RNA Length, and ATP. *Molecular Cell*. **63**, 865–876 (2016).

Acknowledgments:

Data presented are available upon request from EML or ASG; We would like to thank members of the Gladfelter Lab for critical discussions, Erik Griffin, Jamie Moseley, Danny Lew, Mark Peifer, and Henry Higgs for critically reading the manuscript, the HHMI HCIA at the Marine Biological Laboratory in Woods Hole for providing a community to incubate these ideas, Alain Laederach and Lab for pilot experiments and support in initiating RNA analysis and Timothy Straub for useful data analysis discussions; We would also like to thank Tom Christy and Patrick Irving of the Weeks Lab for SHAPE method and analysis help; This work was supported by NIH GM R01-GM081506 to ASG, the HHMI Faculty Scholars program to ASG, NIH

R35 GM122532 to KMW, American Cancer Society Fellowship 130845-RSG-17-114-01-RMC to CW, and NIH 1DP2 GM105453, NIH R01 GM115631 to SM.

Figure 1 Langdon et al.

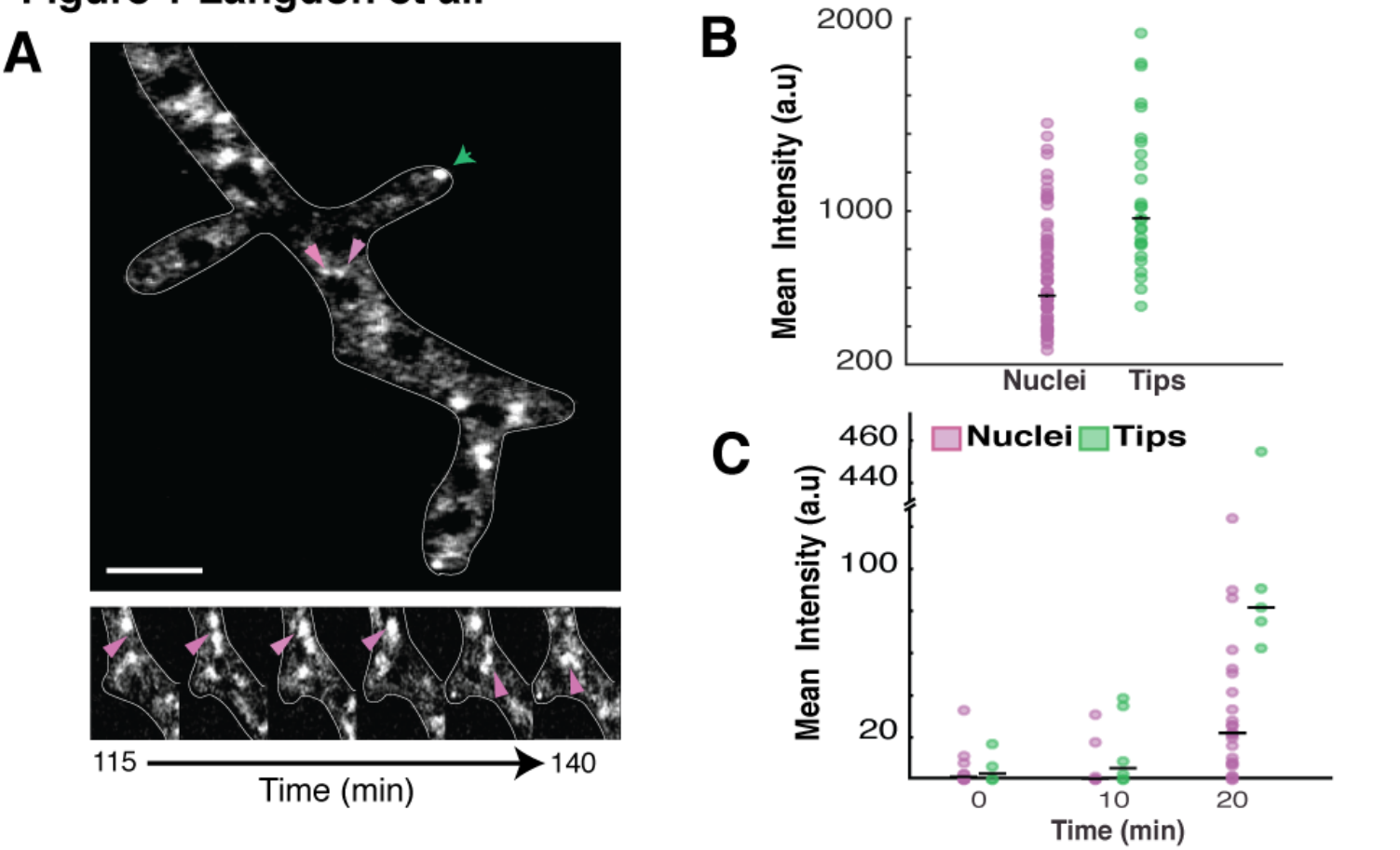

Fig. 1. Whi3-RNA droplets containing different mRNAs are distinct within cells.

A. Above, Representative fluorescent image shows Whi3-tomato condenses into droplets around nuclei and at tips in *Ashbya gossypii*. Green arrows denote a tip droplet and pink arrows denote nuclear associated droplets. Scale bar 5 um. Below, nuclear associated Whi3 droplets (pink arrow) accumulate and fuse over time.

B. Mean intensity of Whi3-tomato is higher in tip droplets (green) than nuclei droplets (pink). N= 70 nuclei and 30 tips. Black bars indicate the medians.

C. Incorporation of JF649 Halo dye into Whi3-Halo droplets at tips is greater than into Whi3-Halo droplets around nuclei over time in N= 40 Nuclei and 15 tips. Black bars indicate the medians.

D. *BNI1* mRNAs (green) and *CLN3* mRNAs (pink) do not co-localize in *Ashbya* cells. In contrast, *BNI1* mRNAs (green) co-localize with *SPA2* mRNAs (pink). The green arrow marks where the two RNAs overlap at the growing tip. Nuclei are labeled in blue. Images are representative of N≥20 cells. Scale bar 5 um. **E.** Quantification of fraction of mRNA co-localized between *BNI1* and *CLN3* or *BNI1* and *SPA2* at either tips or around nuclei. N= 40 tips and nuclei for 20 cells.

Figure 2 Langdon et al.

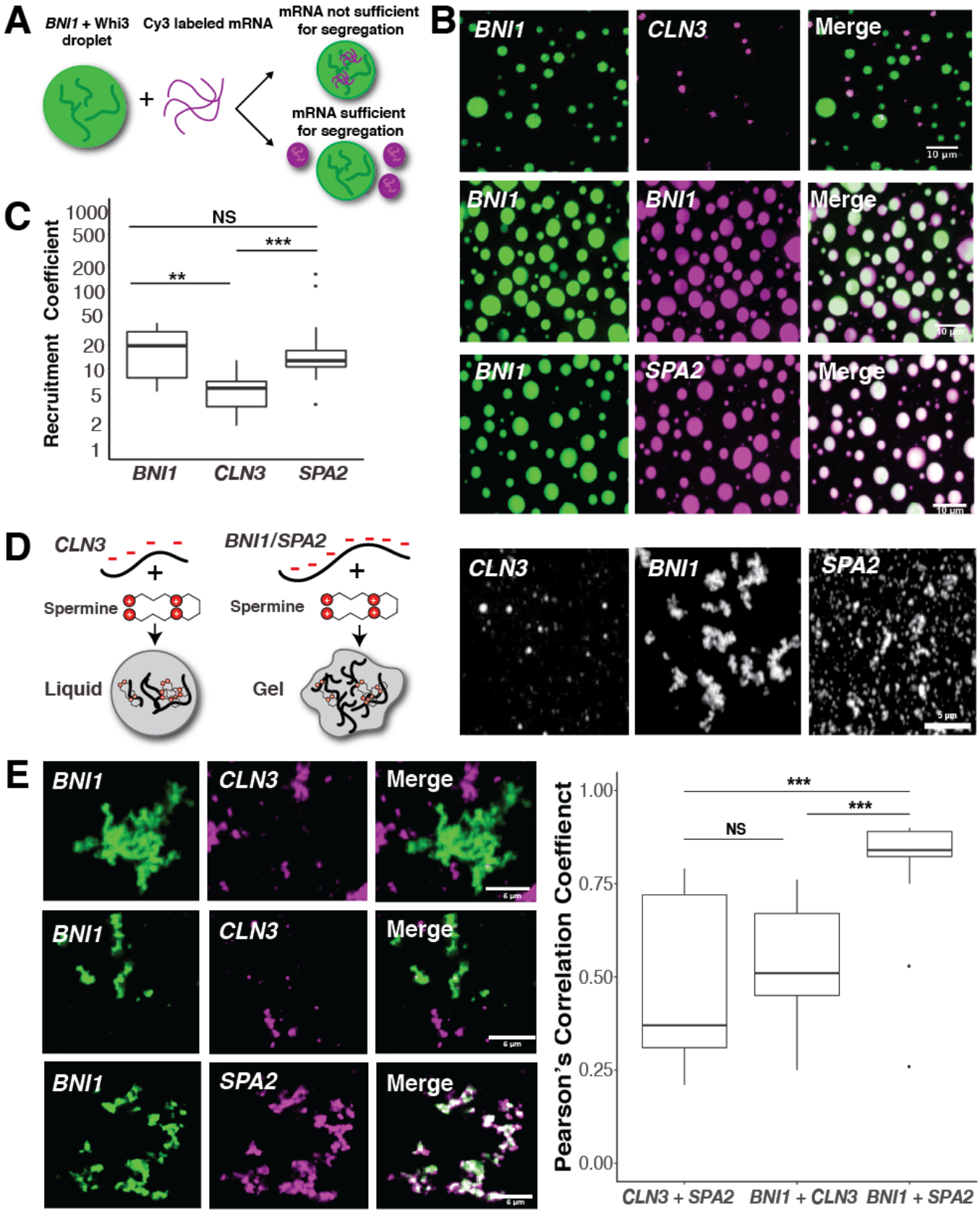

Fig. 2. RNA phase separations segregate based on function in vitro.

A. Experimental schematic of in vitro droplet recruitment assay.

B. Representative images show cy3-labeled *CLN3* mRNA (pink) is not efficiently recruited into Whi3-*BNI1* droplets (green). In contrast, cy3-labeled *BNI1* or *SPA2* mRNA (pink) is recruited into Whi3-*BNI1* droplets (green).

C. Measurement of how much cy3-labeled mRNA is recruited into Whi3-*BNI* droplets from three independent experiments. NS, not significant, $p > 0.05$; **, $p < 0.01$; ***, $p < 0.001$ by unpaired t test.

D. Simplified schematic describing in vitro RNA-only, droplet assay where *CLN3*, *BNI1*, or *SPA2* are incubated with positively charged spermine tetrahydrochloride to induce electrostatic mediated phase separation into liquid or gel-like droplets. Representative images show RNA only assemblies.

E. Representative images showing *CLN3* droplets (pink) are excluded from *BNI1* droplets (green) when the RNAs are mixed in the presence of spermine. In contrast, *BNI1* droplets (green) overlap with *SPA2* droplets (pink).

F. Pearson's Correlation Coefficient in RNA only experiments between *BNI1* and either *CLN3* (left) or *SPA2* (right). *BNI1* and *SPA2* fluorescent signals are significantly more correlated to each other than *BNI1*/*CLN3* and *CLN3*/*SPA2* signals (far left), indicating *CLN3* is still excluded from functionally unrelated assemblies in the absence of Whi3.

Figure 3 Langdon et al.

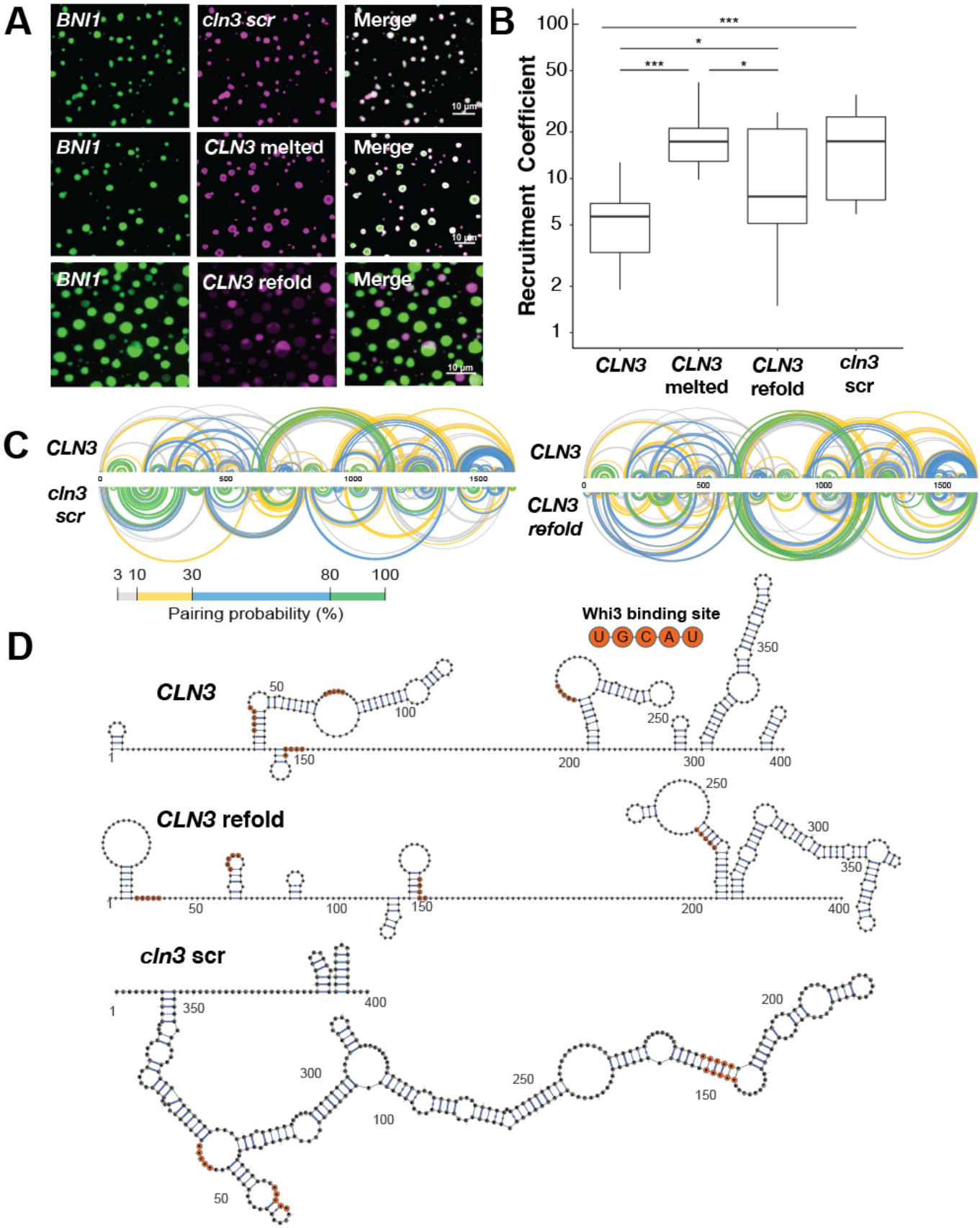

Fig. 3. RNA secondary structure determines specificity of Whi3-*CLN3* droplets.

A. Representative images showing the recruitment of scrambled (*cln3* scr)**,** melted, and refolded (*CLN3* refold) *CLN3* mRNA (pink) into Whi3-*BNI1* droplets (green) (8 uM Whi3, 5 nM RNA).

B. The recruitment coefficients from **A** from three independent experiments. Outliers are indicated with (•) marks. *, $p<0.05$; ***, $p < 0.001$ as determined by unpaired t test.

C. Base-pairing probability compared among *CLN3*, *cln3* scr, and *CLN3* refold. Arcs represent base pairs and are color-coded by probability.

D. Secondary structure models for the first 400 nucleotides of *CLN3*, *CLN3* refold, and *cln3* scr. Whi3 binding sites are denoted in orange.

Figure 4 Langdon et al.

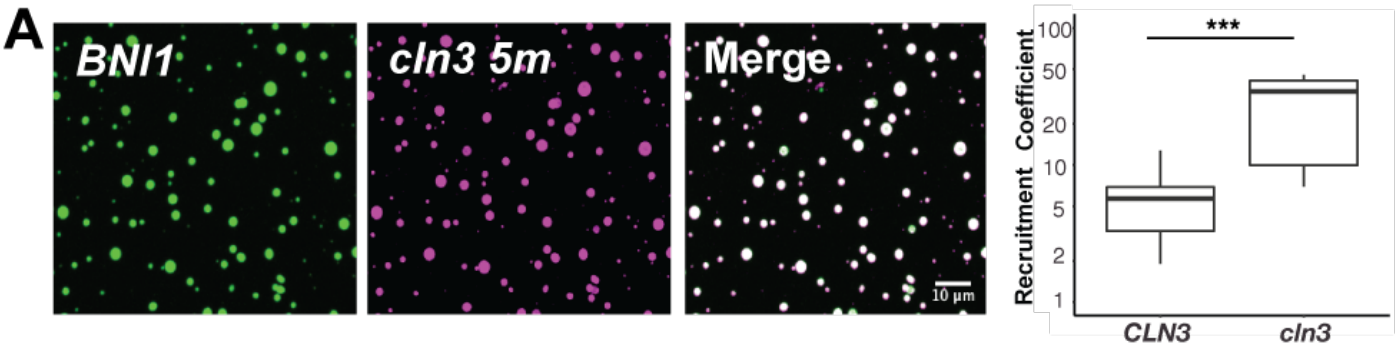

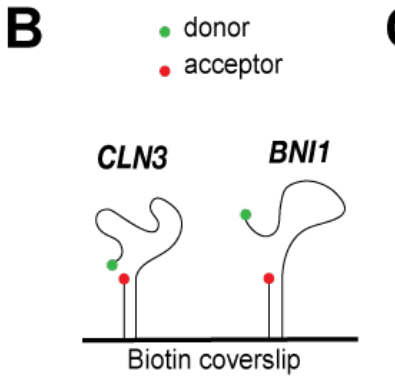

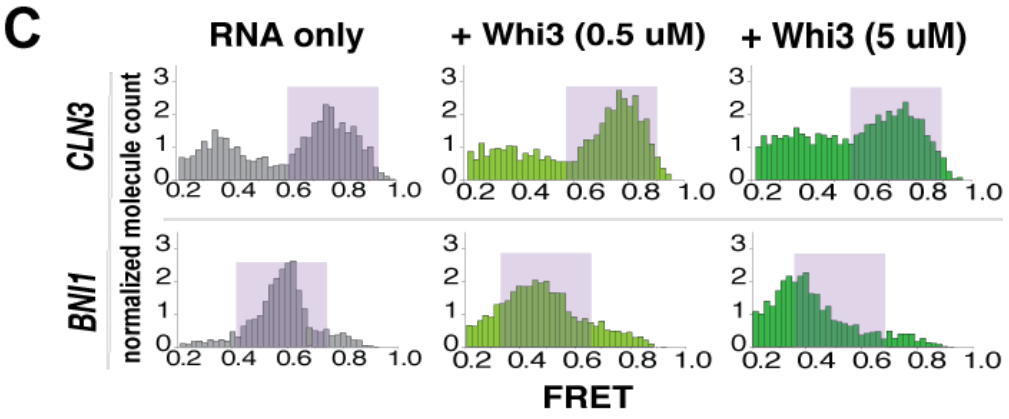

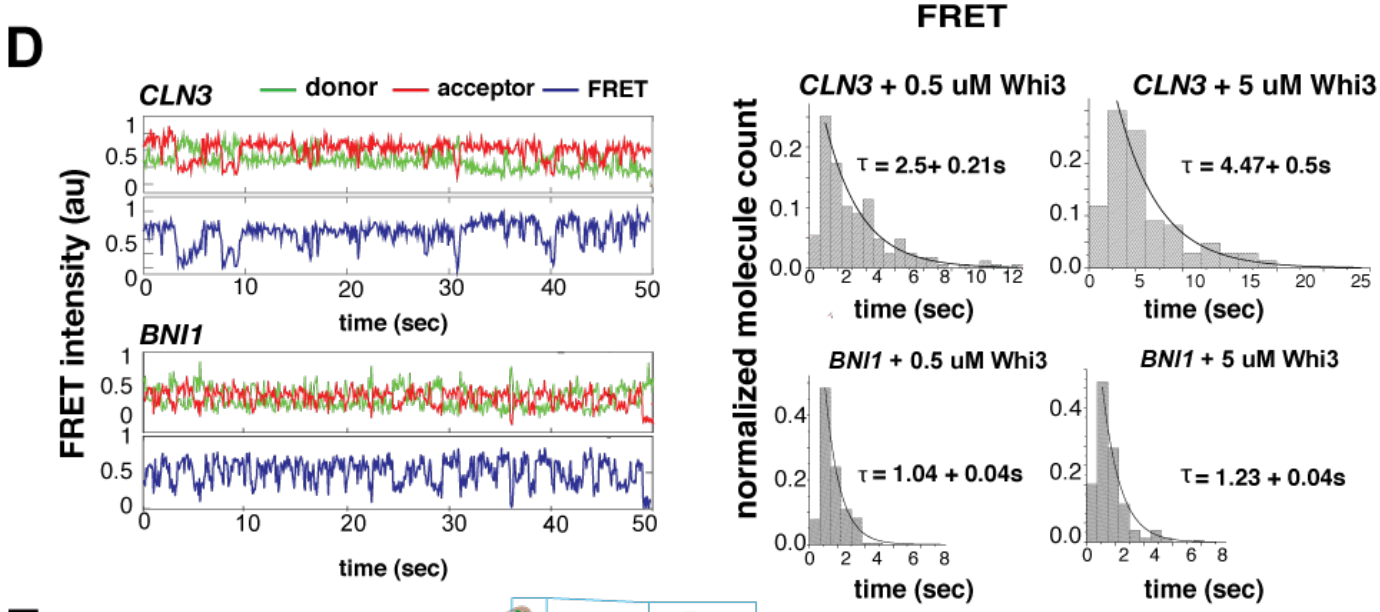

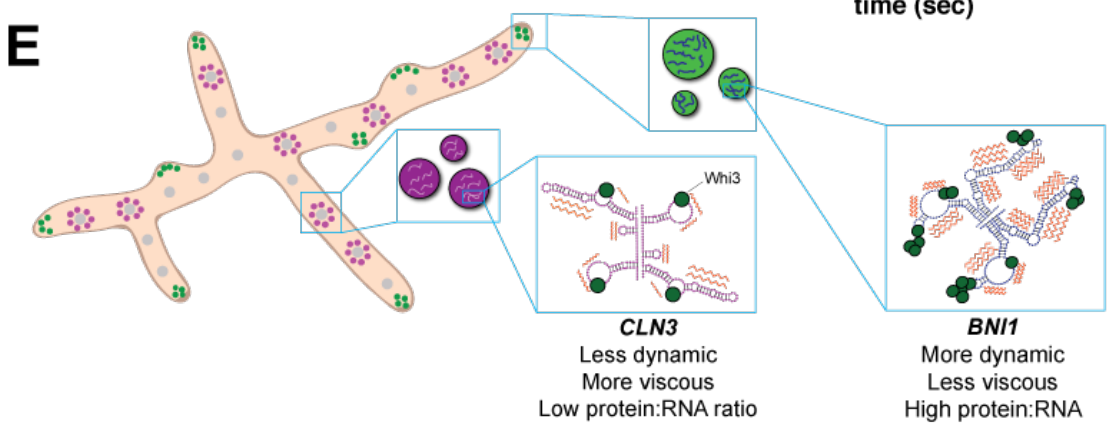

Fig. 4. Whi3 binding alters RNA behavior.

A. Representative images showing the recruitment of the mutant *cln3-5m* mRNA (pink) into Whi3-*BNI1* droplets (green) (8 uM Whi3, 5 nM RNA). Recruitment coefficient of *cln3-5m* shows more efficient RNA recruitment compared to *CLN3* from three independent experiments. *, $p<0.05$; ***, $p < 0.001$ as determined by unpaired t test.

B. RNA substrates composed of truncated *CLN3* or *BNI1* sequences and a Cy5-Cy3 FRET pair are annealed to a Biotin labeled RNA and immobilized on a Biotin coverslip.

C. FRET histograms before (gray) and after (green) 0.5 or 5 uM Whi3 addition. Purple shaded regions denote high and mid FRET states for *CLN3* and *BNI1*, respectively.

D. Averaged cy3 (green), cy5 (red) intensities, and representative FRET traces (blue) obtained from smFRET experiments of *CLN3* and *BNI1* in the presence of 5 uM Whi3. Dwell time analysis shows slower FRET fluctuations for *CLN3* than *BNI1* in the presence of Whi3 (0.5 uM and 5 uM).

E. Proposed model in which RNA secondary structures have been "tuned" to promote the selective uptake of distinct RNAs and protein constituents into droplets leading to diverse dynamics (orange zig-zags) of different droplet complexes

Supplementary Materials:

Materials and Methods

Cell culture and Imaging

Ashbya cells were grown in 10 mL Ashbya full media (AFM) under selection of either G418 (200 ug/ml) or Clonat (100 ug/ml) in a 125 ml baffled flask shaking at 30°C for 16 hours. The cultures were then transferred to 15 ml conical tubes (VWR) for centrifugation at 350 rpm for 2 min. AFM was removed and cells were suspended in 10 ml 2X Low Fluorescence media. Cells were then placed on a 2X Low Fluorescence media gel-pad containing 1% agarose embedded in a depression slides, sealed with valap and imaged. For dye incorporation experiments, Ashbya cells encoding a Whi3 HaloTag were spun down, washed with 2X Low Fluorescence Media and then incubated with 62.5 nM JF649 Halo dye (Lavis Lab, Janelia Farms Research Campus) for 20 min. The cells were then washed twice before being placed on gel pads and imaged at indicated time intervals. All image processing and analysis for in vivo experiments was carried out in either Fiji or MATLAB.

RNA FISH and Imaging

RNA smFISH labeling was performed as previously described(*28*). Briefly, cells were grown overnight at 30 °C in AFM and were fixed using 3.7% (vol/vol) formaldehyde (Fisher Scientific) and then washed twice with cold buffer B. Cells were resuspended in 1mL of spheroplasting buffer and digested using 1.5 mg/ml Zymolyase (MP Biomedicals) for 30 min at 37 °C. Cells

were washed twice with buffer B, and then treated with Proteinase K for 5 min to digest proteins and unmask protein-bound RNAs. Cells were then washed twice before being resuspended in 70% ethanol, and incubated overnight at 4 °C. Cells were washed twice with SSC wash buffer before being resuspended in hybridization buffer containing Tetraethyl rhodamine (TAMARA) or cy5-conjugated RNA FISH probes (Stellaris LGC Biosearch Technologies) complementary to each transcript of interest. Cells were incubated in the dark overnight at 37 °C. After incubation, cells were washed once with wash buffer, incubated with 5 ug/ml Hoechst (Invitrogen) and incubated at room temperature for 30 min before being washed a final time with wash buffer, mounted on glass slides with 20 ul Prolong Gold mounting medium (Invitrogen), sealed with nail polish, and then imaged. Images were de-convolved using 29 iterations of the Lucy-Richardson algorithm on Nikon Elements software and then processed in FIJI.

Analysis of mRNA fraction co-localized

An 8 X 10 ROI was generated at the tips of hyphae or around individual nuclei in merged images. Percent of co-localization was determined by counting the presence of overlapping signal from each of the individual mRNA channels. A total of 40 tips and nuclei were used for analysis and taken across at least 2 biological replicates. mRNAs inside the nucleus were counted and co-localization events inside the nucleus were counted as well.

Recombinant Protein Expression and Purification

Protein purification was performed as previously described(*15*). In brief, full length Whi3 was tagged with an N-terminal 6-Histidine tag and expressed in BL21 *E. coli* (New England Biolabs). For labeled protein, full length Whi3 was tagged with a C-terminal GFP. Cells were lysed in lysis buffer (1.5M KCl, 20 mM Tris pH 8.0, 20 mM Imidazole pH 8, 1 mM DTT, 1 tablet of Roche protease inhibitor cocktail). The supernatant was incubated and passed over a Ni-NTA resin (Qiagen) in gravity columns. The resin was then washed with 10CV lysis buffer and protein was eluted with 6CV elution buffer (150 mM KCl, 20 mM Tris pH 8.0, 200 mM Imidazole pH 8.0,1 mM DTT). The fractions containing Whi3 protein were dialyzed into fresh droplet buffer (150 mM KCl, 20 mM Tris pH 8.0, 1 mM DTT) and measured with Bradford reagent. Aliquots of protein were flash frozen and stored at -80 ºC.

RNA Transcription

The T7 promoter TAATACGACTCACTATAGGG was cloned into the 5' of CLN3, cln3-5m, *BNI1*, and *SPA2*. The *cln3*-scr plasmid was synthesized with the T7 promoter (IDT). Plasmid DNA was digested with restriction enzymes to obtain a linear DNA template that was then transcribed using T7 Hiscribe in vitro transcription kit (NEB) according to manufacturer's instructions. To obtain labeled RNA for imaging, 0.1 ul of 5 mM cy3-UTP or cy5-UTP (GE Healthcare) was added into the transcription reaction. Transcribed RNAs were then DNAse treated, LiCl precipitated, and washed with 85% ethanol before being re-suspended in TE buffer and stored at -80 ºC.

Droplet Assembly and Imaging

Whi3 used in experiments contain 10:1 unlabeled to GFP-labeled protein. For recruitment experiments, Whi3 protein and cy5 labeled *BNI1* RNA were mixed and incubated for four hours in glass chambers (Grace Bio-Labs) at room temperature to desired concentrations in droplet buffer (150 mM KCl, 20 mM Tris pH 8.0, 1 mM DTT). The chambers were pre-treated with 30 mg/mL BSA (Sigma) for 30 minutes. After four hours, a cy3 RNA of interest was added to the wells, mixed, and incubated for 30 min. Imaging of droplets was done either on a spinning disc confocal microscope (Nikon CSU-W1) with VC Plan Apo 60X/1.49 NA oil immersion objective and an sCMOS 85% QE camera (Photometrics) or a custom spinning disk confocal microscope (Nikon Ti-Eclipse equipped with a Yokogawa CSU-X spinning disk module) using a 60X 1.49 NA oil immersion objective and an air-cooled EM-CCD camera. For the RNA melting experiments, RNA was denatured at 95 ºC for three minutes and then immediately added to preformed droplets. For the RNA refolding experiments, RNA was denatured at 95 ºC for three minutes and then cooled down at 1-4 ºC per minute to 37 ºC final temperature in a thermocycler, added to preformed droplets, and imaged immediately. At least five independent imaging areas were analyzed for each condition. Data shown are representative of three or more independent replicates, across at least two RNA and protein preparations.

RNA Spermine experiments and analysis

For RNA spermine experiments, 10 nM in vitro transcribed mRNAs were incubated for 4 hours in Spermine buffer (10 mM Spermine tetrahydrochlroide (Sigma), 20 mM KCl, 10 mM $MgCl_2$) as previously described (*30*) and then imaged on a custom spinning disk confocal microscope (Nikon Ti-Eclipse equipped with a Yokogawa CSU-X spinning disk module) using a 60X 1.49 NA oil immersion objective and an air-cooled EM-CCD camera. Data shown are representative of three or more independent replicates, across at least two RNA preparations.

Images were cropped to 300 x 300 pixels and the middle 11 z stacks. Cy3 and cy5 channels, representing the different RNAs, were split and each channel was background subtracted with a 10-pixel rolling ball. The ImageJ plugin "Coloc 2" (https://imagej.net/Coloc_2) was used to calculate the Pearson's Correlation Coefficient between the two background-subtracted channels. The Wilcoxon Rank Sum test was used to test for statistical significance between *CLN3*/*BNI1*, *BNI1*/*SPA2*, and *CLN3*/*SPA2* experiments.

Analysis of RNA Recruitment

We calculated a Recruitment Coefficient (RC) for RNAs added into preformed Whi3-*BNI1* droplets which is defined by the following equation:

$$\mathrm{RC} = \frac{[\mathrm{RNA}]_{\mathrm{PD}}}{[\mathrm{RNA}]_{\mathrm{O}}}$$

where RC is the recruitment coefficient, $[RNA]_{PD}$ is the concentration of added RNA (cy3) within the preformed droplets, $[RNA]_{o}$ is the concentration of added RNA (cy3) outside the preformed droplets. A higher RC indicates that the RNA is more concentrated in preformed droplets. All image analysis was performed using FIJI. To obtain the concentration of RNA, image channels were split into preformed droplets (cy5) and added RNA (cy3). A mask was created on the preformed droplet channel after background subtraction. Droplets were identified using the 3D objects Counter plugin, with intensity threshold of 1480 for data acquired on the Yokogawa CSU-X and 120 for data acquired on the Nikon CSU-W1. This method was used to obtain the integrated density and the area of the preformed droplets. Average mean fluorescent intensity (MFI) of preformed droplets was then calculated as the sum of integrated density across the z-stack volume divided by sum of area across the z-stack volume. Then, per z-stack volume, inverse selection of preformed droplets is measured for integrated density and area. Average MFI outside preformed droplets calculated as above. MFI values are converted to dye concentration using linear fit of a concentration curve of cy3 dye (one for each instrument). RNA concentration was obtained by normalizing the dye concentration by the average number of dye molecules incorporated into each RNA. To calculate significance between different RNAs, t tests were performed on log-transformed RC values in R version 3.4.

Analysis of Whi3 to RNA ratios

Whi3-RNA droplets were imaged, as previously described, over the course of four hours, starting thirty minutes after the addition of the RNA to Whi3. Image analysis was performed in FIJI. For each time point, the RNA and Whi3 channels were split, background subtracted, and 3D object

counter was used to measure the MFI of both RNA and Whi3 channels separately. MFI values for RNA and Whi3 were then converted to concentrations based on a linear GFP or RNA dye curve. Whi3 concentration was corrected for the unlabeled portion. For each time point, the average concentration was calculated and then the ratio of Whi3 to RNA was calculated as the average Whi3 concentration divided by the average RNA concentration. The standard deviation of the ratio was calculated as follows:

$$SD = \sqrt{\frac{Var(Whi3)}{Whi3^2} - 2 \times \frac{Whi3}{RNA^3} \times Cov(Whi3, RNA) + \frac{Whi3^2}{RNA^4} \times Var(RNA)}$$

where Whi3 is the concentration of Whi3, RNA is the concentration of RNA, Var(x) is the variance of variable x, and Cov (x, y) is the covariance of variables x and y.

SHAPE-MaP experiments and Analysis

SHAPE-MaP was performed as previously described (*31*). In brief, 500 ng of in vitro transcribed RNAS were added to one-ninth volume of 1M7 (10 mM final concentration) or neat DMSO and incubated at room temperature for 10 minutes. RNAs were exchanged into nuclease free water (Ambion) using a desalting column (GE Life Sciences). Modified (1M7) and untreated (DMSO) RNAs were subjected to mutational profiling (MaP) reverse transcription with a random primer (200 ng/ ul R9, NEB). The resulting cDNA were purified (Agencourt RNACLean XP beads, Beckman Coulter) and prepared for library creation by second strand synthesis module (NEB). These cDNAs were then used in amplicon library preparation using Nextera XT indices 1 and 2

and tagamentation and PCR protocol. Sequencing libraries were pooled and then sequenced on an Illumina MiSeq instrument. SHAPE reactivity profiles were created by aligning the RNA reference sequence using ShapeMapper (v1.2, http://chem.unc.edu/rna/software.html). Default parameters were used and the folding module of was not used. RNA structural modeling was performed by Superfold with 1M7 reactivities under default parameters/ software (http://www.chem.unc.edu/rna/software.html) (*34*).

Single Molecule FRET experiments and Analysis.

A custom-built total internal reflection fluorescence (TIRF) microscope was used for all single molecule fluorescence assays. We used lasers of different wavelengths to excite different fluorescent dyes. For FRET experiments involving Cy3 (donor) and Cy5 (acceptor) dyes, we use a solid state 532nm laser (75mW, Coherent CUBE) to excite the donor dye. For the counting of GFP photobleaching steps, we use a 488nm laser (50mW, Coherent Sapphire). For FRET imaging, the emitted signals were separated by dichroic mirrors with a wavelength cutoff of 630nm to separate the Cy3 and Cy5 emissions. The signals are then detected by an EMCCD camera (iXon DU-897ECS0-#BV; Andor Technology) and recorded by the computer. The camera was controlled via custom C++ program, and single molecule traces extracted recorded data using IDL software. Single molecule traces are then displayed and analyzed using Matlab and Origin software. All homemade codes can be found in the single molecule FRET (smFRET) package available at the Center for the Physics of Living Cells (https://cplc.illinois.edu/software/, Biophysics Department, University of Illinois at Urbana-Champaign).

RNA substrate prep

Single strand RNAs are ordered from Integrated DNA Technologies (Coralville, IA, USA) containing amino modifier at the labeling site. The RNAs are labeled using Cy3/Cy5 monofunctional NHS esters (GE Healthcare, Princeton, NJ, USA). 10 nmol of amino modified oligonucleotides in 50 ml of ddH2O and 100 nmol of Cy3/Cy5 NHS ester dissolved in DMSO was added and incubated with rotation overnight at room temperature in the dark. The labeled oligonucleotides were purified by ethanol precipitation[1].

For FRET experiments, *CLN3* and *BNI1* FRET RNA partial duplex RNA substrates are composed of dsRNA consisting of 18bps of random CG-rich sequences and ssRNA consisting of truncated versions of *CLN3* or *BNI1* RNA. A Cy5-Cy3 FRET pair are placed at the junction and the 3' end of the ssRNA, respectively (Fig. 4B).

Following are the sequences for the RNA used:

18mer for *CLN3*: 5' – Biotin – UGG CGA CGG CAG CGA GGC – Cy5 – 3'

CLN3 RNA: 5' – Cy3 – UAC CUG CAC GCG GUC GAG ACG UCU GCA UAC CAA GGA UCA GCC GCU UGC AUU AAA GGG GAC GAA CCG GGG C GCC UCG CUG CCG UCG CCA – 3'

18mer for *BNI1*: 5' – Biotin – ACC GCU GCC GUC GCU CCG – Cy5 – 3'

RNA: 5' – Cy3 – AUA UUC UAC AUG AUU AUG AUG CAU UAG AGA AGG AAA ACG CCU ACU AUA AGU GUU UGA GAG UCC AUA UUC UAC AUG AU CGG AGC GAC GGC AGC GGU – 3'

RNA substrates were annealed by mixing the biotinylated and non-biotinylated oligonucleotides in a 1:2 molar ratio in T50 buffer (50mM NaCl, 10mM Tris-HCl (pH 8.0)). The final concentration of the mixture is at 10uM. The mixture was then incubated at 95°C for 2 minutes followed by slow cooling to room temperature to complete the annealing reaction in just under two hours. The annealed RNAs are diluted to 10nM single molecule stock concentration and stored at -20°C.

All experiments were performed in Whi3 Reaction Buffer (150mM KCl, 50mM Tris-HCl (pH 8.0), 1mM DTT) with an oxygen scavenging system containing 0.8% v/v dextrose, 1 mg/ml glucose oxidase, 0.03 mg/ml catalase, and 10mM Trolox. All chemicals were purchased from Sigma Aldrich (St. Louis, MO). The experiments were all performed at room temperature. 50 to 100pM of biotinylated FRET RNA were immobilized on polyethylene glycol (PEG)-coated quartz surface via biotin-neutravidin linkage.

Whi3-RNA FRET experiment

Whi3 proteins were prepared as described in the method. 0.5 to 5uM of Whi3 proteins in Whi3 Reaction Buffer were added to immobilized RNA substrates.10-20 short movies (10 seconds) and 3-4 long movies (2 minutes) were then taken to monitor the Cy3 and Cy5 emission intensities over time. These are then analyzed to produce the FRET histograms and trajectories shown in Fig. 4C.

Dip-to-dip FRET fluctuation dwell times can be collected between each successive dip in the FRET trace. These time intervals can then be fitted to a single exponential decay function using

Origin (OriginLab Corporation, Northampton, MA) to extract the half-life for each protein-RNA combination.

Author Contribution:

EML designed and performed experiments, analyzed data, prepared figures and drafted manuscript; PB and AN designed and performed experiments, analyzed data, and edited manuscript.; GM performed experiments and analyzed data; CW performed experiments and analyzed data, KMW designed experiments, provided reagents, and edited manuscript. TG provided reagents and edited manuscript. CMT performed experiments. SM designed experiments and edited manuscript. ASG designed experiments, analyzed data, and drafted the manuscript.

Supplemental Figure 1 Langdon et al.

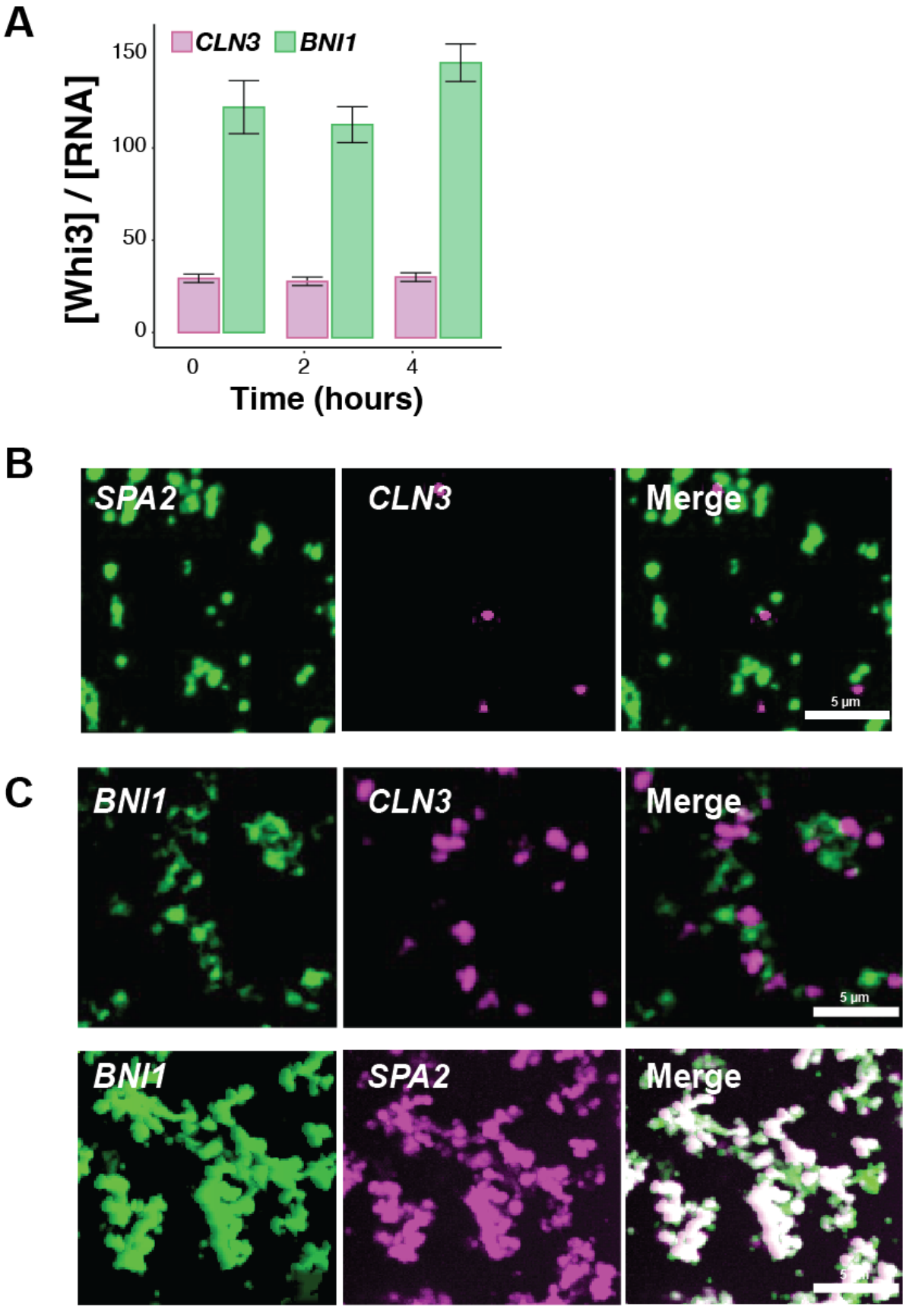

Fig. S1. *CLN3* is excluded from droplets containing polarity mRNAs (*BNI1* or *SPA2*) complexes *in vitro*.

A. Bar plots showing Whi3-*BNI1* droplets (green) incorporate more Whi3 protein over time *in vitro* compared to Whi3-*CLN3* droplets (pink). Data represent two independent experiments.

B. Fluorescent microscopy images show cy3 labeled *CLN3* mRNA (pink) is not efficiently recruited into Whi3-*SPA2* droplets (green) (8 uM Whi3, 5 nM RNA) Images are representative of observations from three independent experiments.

C. Micrographs showing Whi3-*CLN3* droplets (pink) are excluded from Whi3-*BNI1* (green) droplets in 100% yeast extract (140 mg/mL). (Whi3 8 uM, RNA 5 nM). Whi3-*SPA2* droplets (pink) are able to co-condense with Whi3-*BNI1* (green) droplets in 100% yeast extract. (Whi3 8 uM, RNA 5 nM).

Supplemental Figure 2 Langdon et al.

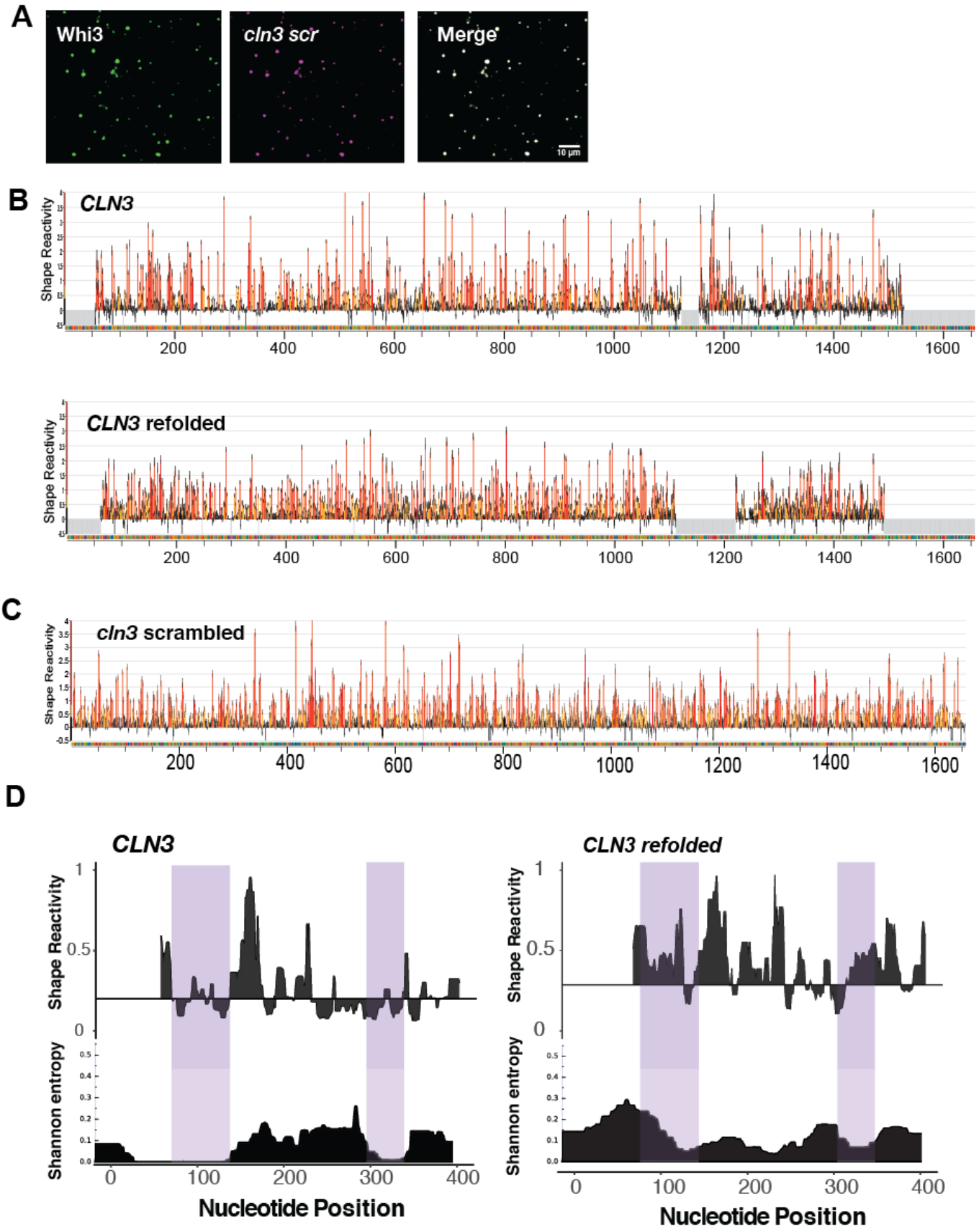

Fig. S2. *CLN3* mRNA secondary structure is altered when the mRNA sequence is scrambled or refolded.

A. Representative images showing the recruitment of *cln3 scrambled* mRNA (5 nM, pink) into normal LLPS with Whi3 (8 uM, green)

B. Shape reactivity profiles for *CLN3* and *CLN3 refolded*. High values indicate many possible structures, while low values suggest a single well-defined structure.

C. SHAPE reactivities and Shannon entropy values for the first 400 nucleotides of the RNAs shown as the median reactivity smoothed over a 19-nt sliding window relative to the global median. The median reactivity (0.19) for *CLN3* in this region is significantly lower than the median reactivity for CLN3 refolded (0.32) suggesting that the *CLN3* refolded mRNA contains less well-defined structures (Wilcoxon rank sum test, $p = 0.001$). Purple shaded regions show low-SHAPE/low-entropy regions. These regions transition to high-SHAPE/high-entropy regions when the *CLN3* sequence is melted and refolded.

Supplemental Figure 3 Langdon et al.

A

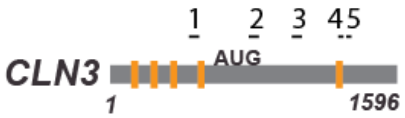

Whi3 binding site

Region	BNI1 start	BNI1 end	CLN3 start	CLN3 end
1	3671	3689	461	479
2	5329	5339	748	758
3	5789	5812	969	992
4	1611	1622	1225	1236
5	948	958	1238	1248

B

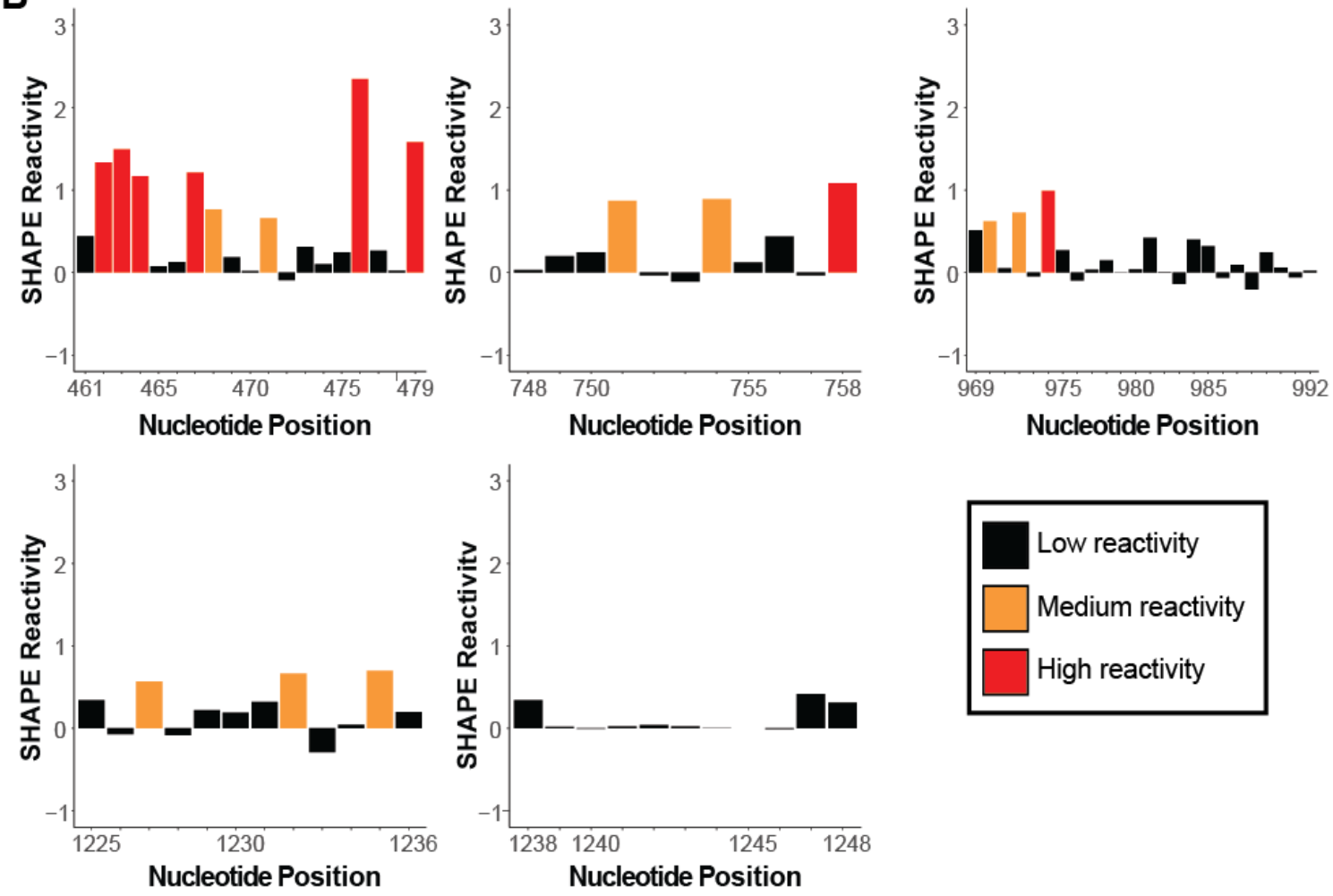

Fig. S3. *CLN3* mRNA contains sequence complementarity regions to *BNI1* mRNA and these regions are located in low-SHAPE/ high-structured regions.

A. Model representation of *CLN3* and *BNI1* mRNA depicting length and valency for Whi3. RNAs are drawn to scale. Whi3 binding sites are denoted in orange and black bars indicate regions of sequence complementarity between the two RNAs. Those regions are also outlined in the table.

B. SHAPE reactivities showing that the 5 regions of complementarity of *CLN3* for *BNI1* occur in low-SHAPE/ high-structured regions.

Supplemental Figure 4 Langdon et al.

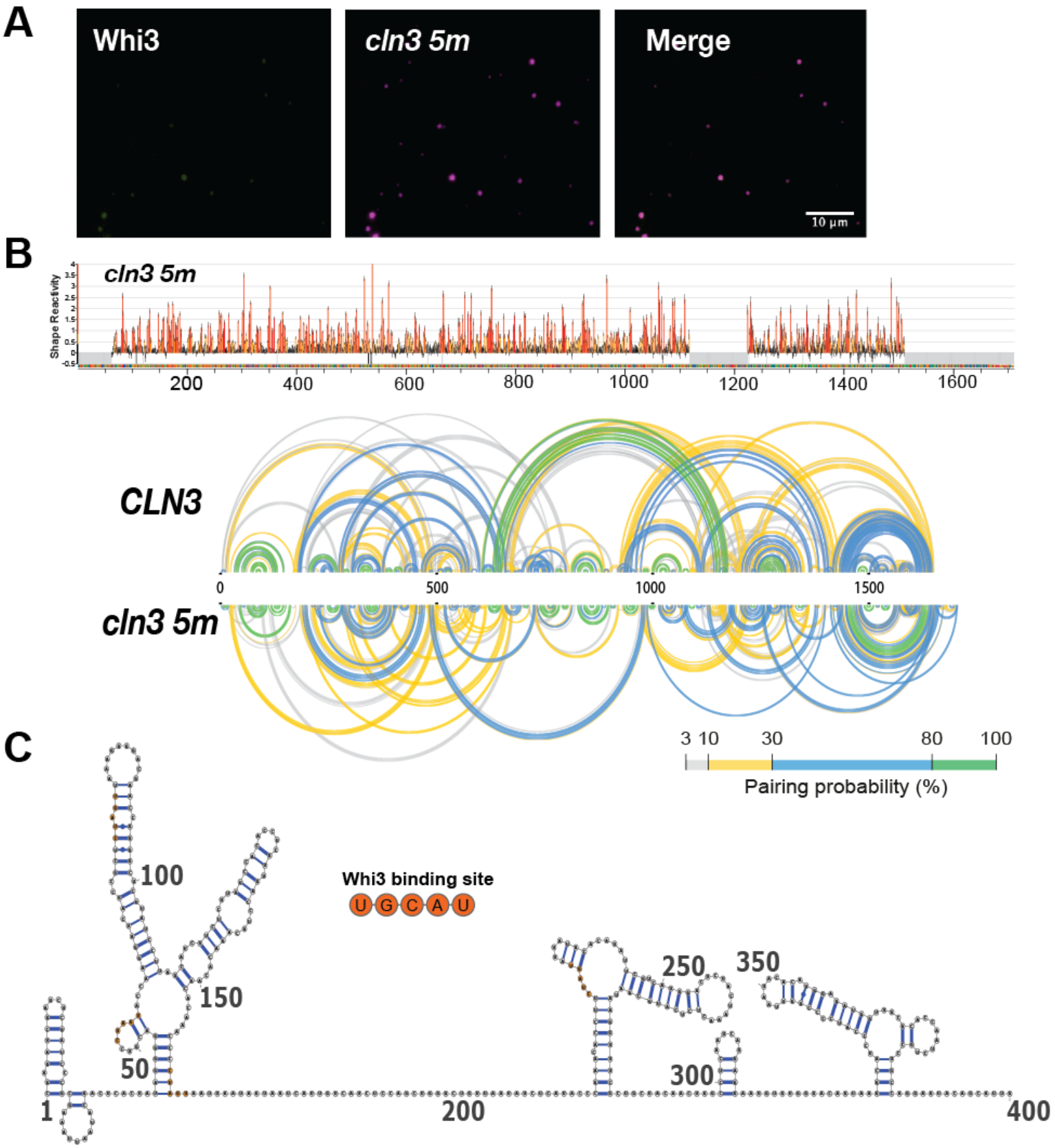

Fig. S4. *cln3 5m* cannot form liquid droplets with Whi3 and has an altered secondary structure.

A. Representative images showing *cln3 5m* mRNA (5 nM, pink) forms RNA only aggregates that do not form LLPS with Whi3 (8 uM, green)

B. SHAPE reactivity profiles for *cln3 5m* and base-pairing probability compared among *CLN3* and *cln3 5m*. Arcs represent base pairs and are color-coded by probability.

C. Secondary structure models for the first 400 nucleotides of *cln3 5m*. Whi3 binding sites are denoted in orange.

Movie S1

Whi3 forms phase separated droplets clustered around nuclei and growing tips in *Ashbya* cells; the droplets undergo fusion events. Related to Fig. 1A. An *Ashbya* hyphae with Tomato-tagged Whi3 visualized with confocal microscopy over 4 hours.